

Acta Radiologica

Draft Manuscript for Review

Radiation-induced Cardiotoxicity in Hypertensive Salt-Sensitive Rats. A Feasibility Study

| | |
|------------------|--|
| Journal: | <i>Acta Radiologica</i> |
| Manuscript ID | SRAD-2023-0844 |
| Manuscript Type: | Original Article |
| Keywords: | cardiac mri, Hypertension < Topics, cardiotoxicity, radiation therapy, myocardial strain |
| | |

SCHOLARONE™
Manuscripts

1
2
3
4
5
6
7
8
9
10
11
12
13
14
15
16
17
18
19
20
21
22
23
24
25
26
27
28
29
30
31
32
33
34
35
36
37
38
39
40
41
42
43
44
45
46
47
48
49
50
51
52
53
54
55
56
57
58
59
60

**Radiation-induced Cardiotoxicity in Hypertensive Salt-Sensitive Rats. A
Feasibility Study**

For Peer Review Only

Abstract

Background: Radiation therapy (RT) plays a vital role in managing thoracic cancers, though it can lead to adverse effects, including significant cardiotoxicity. Understanding the risk factors like hypertension in RT is important for patient prognosis and management.

Purpose: To investigate the impact of RT on cardiotoxicity in hypertensive rats.

Material and Methods: A Dahl salt-sensitive (SS) female rat model was used to study hypertension effect on RT-induced cardiotoxicity. Rats were fed a high-salt diet to induce hypertension and then divided into RT and sham groups. The RT group received 24 Gy of whole-heart irradiation. Cardiac function was evaluated using magnetic resonance imaging (MRI) and blood pressure measurements at baseline, 8-weeks and 12-weeks post-RT. Histological examination was performed after the last timepoint or animal death.

Results: The hypertensive RT rats, at 12-weeks post-RT, demonstrated significant decreases in left-ventricular ejection fraction (EF) ($45\pm 7.2\%$) compared to sham ($68\pm 7.3\%$). Furthermore, circumferential (Ecc) and radial (Err) myocardial strains were significantly reduced compared to sham (Ecc: $-7.4\pm 2.0\%$ RT rats vs. $-11\pm 2.4\%$ for sham; Err: $15\pm 6.5\%$ for RT rats vs. $23\pm 8.9\%$ for sham). Histological analysis revealed significant pathophysiological remodeling post-RT, including nuclear size, interstitial fibrosis, necrosis, and the presence of inflammatory cells.

Conclusion: This study provides valuable insights into the cardiotoxic effects of RT in the context of hypertension, highlighting the potential of using MRI for improved risk assessment with potential for future clinical translation.

Key words: Cardiac MRI, Hypertension, Cardiotoxicity, Radiation Therapy, Myocardial Strain

Introduction

The increasing prevalence of cancer and advancement in treatment methods have led to a growing number of patients receiving radiation therapy (RT) (1-3), especially lung cancer patients commonly undergo RT as a crucial part of their treatment plan, which has been proven to enhance local control and survival (2, 4-6). Despite treatment advancements improving survival, the radiation effect on the heart remains a major concern (2, 7, 8). As cardiac dysfunction can progress to heart failure if not appropriately managed (2, 3, 5, 9, 10), the identification of sensitive, non-invasive biomarkers for the early detection of subclinical cardiac dysfunction is crucial to reduce the morbidity and mortality associated with thoracic RT.

RT-induced cardiotoxicity can manifest in various forms, ranging from mild to severe, including but not limited to, pericarditis (6, 11-13), coronary artery disease (6, 13-16), valvular heart disease (6, 13, 17), and myocardial dysfunction (6, 13, 18-20). While numerous studies have focused on the effects of radiation dose and the volume of the heart exposed to radiation on the development of cardiotoxicity (2, 7, 21, 22), the effect of major baseline risk factors on RT-induced cardiotoxicity is not fully elucidated. Specifically, hypertension is a prevalent and well-established risk factor in lung cancer patients (23-26). Recent evidence suggests that hypertension may play a significant role in the development of RT-induced cardiotoxicity (21, 27-30). Hypertensive patients may have an increased vulnerability to RT-induced damage to the heart, potentially exacerbating the risk of cardiotoxicity (1, 2, 21, 23, 25).

We have previously studied the effect of RT on normotensive rats (31). In this study, we further investigate the incremental effect of hypertension on RT-induced cardiotoxicity in the same animal model. The pilot results from this study have the potential studies on humans towards enhancing the management of cardiotoxicity risks and improving outcomes in cancer patients.

Material and Methods

Animal Model and Irradiation Procedure

The study (Fig. 1) was approved by the institutional animal care committee of the Medical College of Wisconsin. Dahl salt-sensitive (SS) rats, which have been extensively used in the investigation of hypertension and cardiac complications (32-35), were used in this study. Inbred SS female rats (n=6) were administered a standard low-salt diet (0.4% NaCl) from 3 to 6 weeks of age (36). To induce hypertension, the rats were fed high-salt diet (4% NaCl) from 6 to 10 weeks of age, after which they resumed a low-salt diet (32, 33, 37, 38).

At 10 weeks of age, the rats were randomly allocated to two groups: RT group (n=4) and sham non-irradiated group (n=2). The RT group underwent whole-heart irradiation with a dose of 24Gy, guided by onboard cone beam computed tomography for precise targeting (one anterior-posterior beam and two lateral beams, 225kVp, 13mA, and clockwise gantry rotation direction) (39). The dose rate was 2.72Gy/min, administered using high-precision image-guided X-RAD SmART irradiator (Precision X-Ray, North Branford, CT). Fig 2 shows dose distribution in different organs.

Blood pressure, including systolic blood pressure (SBP), diastolic blood pressure (DBP), and pulse, was measured using a tail-cuff Visitech system at the same timepoints of the MRI scans.

MRI Scans and Image Analysis

The rats were imaged on a small-animal 9.4T MRI scanner (Bruker, Rheinstetten, Germany). The MRI scan included both cine and tagged images acquired (40, 41) along with a full stack of short-axis (SAX) and long-axis (LAX) cine slices covering the whole left ventricle (LV). Three SAX-tagged slices (basal, mid-ventricular, and apical) were acquired in addition to LAX slices.

1
2
3 The cine sequence imaging parameters were as follow: repetition time (TR) = 6.25ms, echo time
4 (TE) = 2.2ms, flip angle = 15°, matrix = 176×176, slice thickness = 1mm, bandwidth =
5
6 526Hz/pixel, scan time ~2 min/slice. The tagging sequence imaging parameters were similar to
7
8 cine imaging, except for the following: TE = 2.5ms, matrix = 256×256, bandwidth =
9
10
11
12 375Hz/pixel, scan time = 4-5min/slice (40).
13
14

15 Cine image processing was conducted using the cvi42 software (Circle Cardiovascular Imaging,
16
17 Calgary, Canada). The measurements from all the SAX slices were used to evaluate global
18
19 cardiac functions including end-diastolic volume (EDV), end-systolic volume (ESV), stroke
20
21 volume (SV), ejection fraction (EF), and mass.
22
23
24

25 The tagged images were analyzed using the sinusoidal modelling technique (42, 43) (InTag,
26
27 Lyon, France) to measure the circumferential (Ecc), radial (Err), and longitudinal (Ell) strain.
28
29 The analysis was performed on the SAX images acquired at the basal, mid-ventricular, and
30
31 apical levels and on the LAX images. Strain analysis was repeated by the same observer (>2
32
33 months) and by another observer to assess data reliability.
34
35
36

37 *Histological Analysis*

38
39 The hearts were harvested from fully anesthetized RT and sham rats at 12-weeks post-RT or at
40
41 the time of death. The isolated hearts were handled using standard procedures (44). Fixed tissue
42
43 samples were embedded in paraffin with sections taken at SAX levels from the basal, mid-
44
45 ventricular, and apical regions of the LV. Four-micrometer sections were cut from each block
46
47 and stained with hematoxylin and eosin (H&E) and Masson's trichrome, according to standard
48
49 methods. Furthermore, for mast cell staining, slides were first deparaffinized using Xylene and
50
51 subsequently rehydrated through descending concentrations of ethanol. Each slide was covered
52
53
54
55
56
57
58
59
60

1
2
3 in a 0.1% toluidine blue in 1% sodium chloride (pH 2.0) for 3 minutes. Image acquisition
4
5 utilized a Nikon Eclipse 50i upright microscope, with eighteen images from each level (basal,
6
7 mid-ventricular, and apical) cropped for mast cell staining. Quantification was done by counting
8
9 mast cells per high-power field by a trained pathologist.
10
11

12 13 *Statistical Analysis* 14

15 Descriptive statistics were calculated for all measured variables, which include SBP, DBP, pulse,
16
17 EDV, ESV, SV, EF, mass, Ecc, Err, and Ell. Data are expressed as the mean \pm standard deviation
18
19 (SD). Because of small sample size, a non-parametric test, Mann-Whitney U test, was applied for
20
21 all variables with $p < 0.05$ considered significant. Bland-Altman analysis (45) was conducted to
22
23 assess intra-observer and inter-observer variabilities in the generated measurements.
24
25
26
27
28
29
30
31
32
33
34
35
36
37
38
39
40
41
42
43
44
45
46
47
48
49
50
51
52
53
54
55
56
57
58
59
60

Results

Physiological Results and Cardiac MRI

The hypertensive rats developed high blood pressure at baseline (33, 34), persisting throughout the experiment (Table 1), compared to the lower blood pressure observed in low-salt diet rats (23, 25, 35, 38, 46). At baseline, both sham and RT groups had high SBP and DBP. By 8-weeks post-RT/sham, the sham group showed increased SBP, unlike the stable RT group. At 12-weeks, the sham group's SBP and DBP significantly rose, while the RT group's SBP decreased and DBP declined noticeably. As for the pulse rate, the sham group demonstrated a higher pulse rate compared to the RT group. This trend persisted at 8-weeks post-RT, with the sham group showing an increase and the RT group a slight increase. Interestingly, by 12-weeks post-RT, the sham group's pulse slightly decreased, and the RT group further decreased.

EDV was similar for both groups at baseline. As the study progressed to 8-weeks post-RT, both groups exhibited an increase. By the 12-weeks post-RT evaluation, both groups maintained nearly equivalent EDV levels. ESV initially was slightly lower in the sham group compared to the RT group at baseline. By 8-weeks post-RT, the sham group had a minimal rise in ESV, but the RT group observed a decrease. By the 12-weeks post-RT, the RT group exhibited a significant increase in ESV. Regarding SV, baseline measurements were close between the sham and RT groups. By 8-weeks post-RT, there was an evident increase in both groups. But at the 12-weeks post-RT timepoint, the patterns diverged, with the sham group maintaining its SV while the RT group showing a decrease. Baseline assessments revealed comparable EF values in the two groups. By 8-weeks post-RT, EF in the RT group and sham group increased and slightly increased, respectively. At 12-weeks post-RT, EF in the sham group decreased, whereas it significantly declined in the RT group. At baseline, both sham and RT groups had comparable

1
2
3 mass measurements. By 8-weeks post-RT, both groups exhibited an increase in mass, with this
4 trend continuing through 12-weeks post-RT, where the mass measurements remained closely
5 aligned between the two groups.
6
7

8
9
10 At baseline, both the sham and RT rats exhibited similar strain measurements across Ecc, Err,
11 and Ell as depicted in Fig. 3. The Ecc values for both groups were in close proximity. By 8-
12 weeks post-RT, the sham group slightly increased, whereas the RT rats showed a sharper
13 decrease. This disparity became more evident by the 12-weeks mark, with the sham group
14 ascending further and the RT group settling. For Err, the baseline values were closely matched.
15 This close range persisted at 8-weeks post-RT. Yet, by 12-weeks post-RT, both groups exhibited
16 a rise. Lastly, Ell measurements for both the sham and RT groups were similar at baseline. By 8-
17 weeks post-RT, a subtle decrease was noted in both groups. However, the 12-weeks post-RT
18 measurement revealed a consistent trend while the sham group remained close to its previous
19 value, but the RT group showed a noticeable drop.
20
21
22
23
24
25
26
27
28
29
30
31
32
33

34 To ascertain if there was a significant difference in the distributions of the variables between the
35 sham and RT groups, we performed the Mann-Whitney U test. Despite observing variations in
36 the trends of physiological and MRI parameters between the groups, the Mann-Whitney U test
37 revealed no statistically significant difference between the groups for all the variables
38 considered. The Bland-Altman analysis revealed low intra- and inter-observer variabilities in the
39 strain measurements (Ecc, Err, and Ell), with almost all measurement differences lying within
40 the agreement range of $\text{mean} \pm 2\text{SD}$ of the measurement differences (Fig. 4).
41
42
43
44
45
46
47
48
49
50
51
52
53
54
55
56
57
58
59
60

Histopathologic Results

Fig. 5 demonstrate survival data in the studied rats. Initially, the sham group comprised two rats, and the RT group had four rats. By 11-weeks post-RT, complications following a seizure led to the euthanasia of one rat from the sham group, and another rat from the RT group had died. At 12-weeks post-RT, two rats from the RT group had developed heart failure and were consequently euthanized. Another rat from the same group died during the blood pressure measurement. Finally, one sham rat was euthanized at the 12-weeks post-RT.

Multiple fields of view from myocardial tissue sections of the sham and RT groups were examined. Specifically, for each staining method employed, 26 fields of view were analyzed for the sham group and 78 for the RT groups. These fields of view represent zoomed and cropped images of stained myocardial tissues. H&E staining demonstrated distinct differences in myocardial tissue organization between the sham and RT groups (Fig. 6). The RT group exhibited a more subtle pink staining color in H&E staining process, which could potentially signify a reduction in the concentration of cytoplasmic proteins. Compared to the sham group, which shows well-organized and normal histoarchitecture, the RT group exhibits several histopathological changes. These include increased nuclear size, interstitial fibrosis and necrosis, heightened capillary density, the presence of inflammatory cells, and sarcoplasmic vacuolation (Fig. 6). RT-induced damage can manifest as a chronic process, marked by the collagen deposition and excessive production of fibrosis. The levels of fibrosis were assessed in myocardial tissue of the hypertensive rats in both sham and RT groups using Masson's trichrome staining (Fig. 7). Upon employing Masson's trichrome staining, areas indicative of tissue damage, including areas of fibrosis, necrosis, and augmented extracellular matrix components were detected in the myocardial tissue. The analysis revealed comparable fibrosis levels in both

1
2
3 groups, with the sham group averaging $1.65 \pm 1.86\%$ and the RT group at $1.56 \pm 0.94\%$. The
4
5 difference in fibrosis levels between the groups was not statistically significance (p-value=0.72).
6
7 Additionally, the toluidine blue staining revealed a significant increase in mast cell infiltration
8
9 within the LV in the RT group as compared to the sham group (p-value<0.05) (Fig. 8).
10
11
12
13
14
15
16
17
18
19
20
21
22
23
24
25
26
27
28
29
30
31
32
33
34
35
36
37
38
39
40
41
42
43
44
45
46
47
48
49
50
51
52
53
54
55
56
57
58
59
60

For Peer Review Only

Discussion

In this study, we investigated RT's impact on cardiac function in hypertensive rats, utilizing MRI and histological analysis to assess alterations in cardiac parameters and pathology. The results demonstrated significant changes in cardiac function as evidenced by both histology and strain measurements.

The hypertensive rats maintained elevated levels of blood pressure throughout the study. At 8-weeks post-RT, the rats showed stable levels of both SBP and DBP, while the sham group experienced an increase. Furthermore, a post-RT increase in pulse rate was observed in both RT and sham groups, although the sham group maintained a higher pulse rate.

Baseline EF values were comparable between sham and RT rats. A moderate increase in EF was seen in the sham group at 8-weeks post-RT while the RT group exhibited a pronounced increase at the same timepoint. Both Ecc and Err strains were found to decrease (in absolute value) at 8-weeks post-RT compared to the sham group. However, we noted an unexpected increase in strains at 12-weeks post-RT in the hypertensive rats. The variation in strain patterns in the hypertensive rats in this study compared to previously reported results in similar normotensive rats (41) could reflect the complex interactions between hypertensive conditions and RT.

Hypertension is known to induce alterations in the myocardial structure and function (23, 25, 47), which might influence the cardiac response to radiation. Therefore, myocardium strain changes may be indicative of a compensatory behavior in the hypertensive rats.

The histopathological analysis using H&E staining revealed distinct differences in myocardial tissue organization between the sham and RT groups, highlighting the structural modifications effect of RT on the myocardium. Observations from Masson's trichrome staining revealed a

1
2
3 higher level of fibrosis in myocardial tissue upon irradiation although the differences were not
4 statistically significant when compared to the sham group. Notably, the toluidine blue staining
5 exhibited a statistically significant difference between two groups, indicating mast cell
6 infiltration. Mast cells are known to be involved in inflammation and fibrosis and may play a
7 pivotal role in mediating RT-induced cardiac changes.
8
9
10
11
12
13

14
15 In comparing irradiated hypertensive rats to previously reported irradiated normotensive rats (31)
16 (Fig. 9), significant differences in cardiac responses to RT were observed. Hypertensive rats
17 displayed a pronounced hypertrophic response with substantially increased cardiac mass,
18 diverging from the gradual increase seen in normotensive rats. This highlights the impact of
19 hypertension on pathological cardiac remodeling.
20
21
22
23
24
25

26
27 Both groups initially showed an EF increase post-RT, but by the 10/12-weeks post-RT, the
28 hypertensive group experienced a substantial EF decrease, while the normotensive group
29 sustained their elevated levels. This suggests an exacerbated vulnerability of the hypertensive
30 myocardium to radiation.
31
32
33
34
35

36
37 The changes in Ecc, Err, and Ell between groups at varying stages underscore the differential
38 myocardial response to radiation in the presence of hypertension. Especially compelling are the
39 robust correlations among these strain parameters within the hypertensive group. Even the
40 normotensive group's distinct correlation between mass and Ecc, could indicate a radiation-
41 induced myocardial stress response that is hypertensive-independent.
42
43
44
45
46
47
48

49 Our findings, compared with data on normotensive rats (31, 41), highlights hypertension's
50 modulatory role on cardiac response to radiation. The hypertensive rats exhibited hyperkinetic
51 behavior at the third timepoint, diverging from the decreasing trend in normotensive rats,
52
53
54
55
56
57
58
59
60

1
2
3 aligning with findings from the hypertensive SS rat model (37, 48, 49). These comparisons
4
5 underline the importance of developing tailored therapeutic strategies and risk assessments for
6
7 hypertensive patients undergoing RT, considering their distinct cardiac adaptation to RT.
8
9

10
11 The study has limitations. First, the small sample size may limit the statistical power and
12
13 generalizability of the results. Nevertheless, the results clearly demonstrate different contractility
14
15 patterns in the hypertensive rats compared to normotensive rats, which emphasizes the
16
17 incremental RT-induced cardiac damage in the presence of hypertension.
18
19

20
21 Despite a slight difference in last follow-up timepoint between the hypertensive and
22
23 normotensive rats (31), our results clearly demonstrated a worse effect of baseline hypertension
24
25 on cardiac function than RT alone. The time course of RT-induced cardiac damage is crucial; for
26
27 instance, the decreasing strain in normotensive rats from 8-weeks to 10-weeks post-RT suggests
28
29 progressive decline due to cumulative radiation effects. Conversely, the increased strain at 12-
30
31 weeks post-RT in hypertensive rats might indicate potential regional hyperkinetic contractility
32
33 despite reduced EF, which warrants further investigation in future larger studies.
34
35

36
37 Another limitation is this study was constrained to observations up to 12-weeks post-RT,
38
39 potentially overlooking longer-term RT effects, particularly with baseline hypertension.
40
41

42
43 Nevertheless, previous studies demonstrated continued deterioration in EF in this rat model
44
45 which results in heart failure by the 20th week post-RT (39).
46

47
48 In conclusion, this pilot study provided valuable insights into the effects of RT on hypertensive
49
50 rats, offering a more clarification of how RT might interact with hypertension to escalate
51
52 cardiotoxicity. MRI findings indicate significant deterioration of myocardial contractility
53
54 following RT, as demonstrated by decreased LV EF and strain measurements and confirmed by
55
56
57
58
59
60

1
2
3 histopathological analysis. The promising results from this study underscore the damaging
4
5 impact of RT on cardiac function, particularly in the presence of hypertension, which has
6
7 potential translational by conducting clinical trial for better treatment management and improved
8
9 outcomes in cancer patients receiving RT.
10
11
12
13
14
15
16
17
18
19
20
21
22
23
24
25
26
27
28
29
30
31
32
33
34
35
36
37
38
39
40
41
42
43
44
45
46
47
48
49
50
51
52
53
54
55
56
57
58
59
60

For Peer Review Only

References

1. Baskar R, Lee KA, Yeo R, et al. Cancer and radiation therapy: current advances and future directions. *Int J Med Sci* 2012;9(3):193.
2. Darby SC, Cutter DJ, Boerma M, et al. Radiation-related heart disease: current knowledge and future prospects. *Int J Radiat Oncol Biol Phys* 2010;76(3):656-65.
3. Henson K, McGale P, Taylor C, et al. Radiation-related mortality from heart disease and lung cancer more than 20 years after radiotherapy for breast cancer. *Br J Cancer* 2013;108(1):179-82.
4. Yaromina A, Krause M, Baumann M. Individualization of cancer treatment from radiotherapy perspective. *Mol Oncol* 2012;6(2):211-21.
5. Badiyan SN, Puckett LL, Vlacich G, et al. Radiation-Induced Cardiovascular Toxicities. *Curr Treat Options Oncol* 2022;23(10):1388-404.
6. Belzile-Dugas E, Eisenberg MJ. Radiation-induced cardiovascular disease: Review of an underrecognized pathology. *J Am Heart Assoc* 2021;10(18):e021686.
7. Erven K, Florian A, Slagmolen P, et al. Subclinical cardiotoxicity detected by strain rate imaging up to 14 months after breast radiation therapy. *Int J Radiat Oncol Biol Phys* 2013;85(5):1172-8.
8. Herrmann J. Adverse cardiac effects of cancer therapies: cardiotoxicity and arrhythmia. *Nat Rev Cardiol* 2020;17(8):474-502.
9. Pedersen LN, Schiffer W, Mitchell JD, et al. Radiation-induced cardiac dysfunction: Practical implications. *Kardiol Pol* 2022.

10. Zhu D, Li T, Zhuang H, et al. Early Detection of Cardiac Damage by Two-Dimensional Speckle Tracking Echocardiography after Thoracic Radiation Therapy: Study Protocol for a Prospective Cohort Study. *Front Cardiovasc Med* 2022;8:2271.
11. Imazio M, Colopi M, De Ferrari GM. Pericardial diseases in patients with cancer: contemporary prevalence, management and outcomes. *Heart* 2020;106(8):569-74.
12. Szpakowski N, Desai MY. Radiation-associated pericardial disease. *Curr Cardiol Rep* 2019;21:1-10.
13. Wang H, Wei J, Zheng Q, et al. Radiation-induced heart disease: a review of classification, mechanism and prevention. *Int J Biol Sci* 2019;15(10):2128.
14. Carlson LE, Watt GP, Tonorezos ES, et al. Coronary artery disease in young women after radiation therapy for breast cancer: the WECARE Study. *Cadio Oncol* 2021;3(3):381-92.
15. da Silva RMFL. Effects of radiotherapy in coronary artery disease. *Curr Atheroscler Rep* 2019;21:1-8.
16. Kirresh A, White L, Mitchell A, et al. Radiation-induced coronary artery disease: a difficult clinical conundrum. *Clin Med* 2022;22(3):251.
17. Aluru JS, Barsouk A, Saginala K, et al. Valvular Heart Disease Epidemiology. *Medical Sciences* 2022;10(2):32.
18. Cutter DJ, Darby SC, Yusuf SW. Risks of heart disease after radiotherapy. *Tex Heart Inst J* 2011;38(3):257.
19. Darby SC, Ewertz M, McGale P, et al. Risk of ischemic heart disease in women after radiotherapy for breast cancer. *N Engl J Med* 2013;368(11):987-98.
20. Donnellan E, Phelan D, McCarthy CP, et al. Radiation-induced heart disease: A practical guide to diagnosis and management. *Cleavel Clin J Med* 2016;83(12):914-22.

- 1
2
3 21. Blinded for anonymity
- 4
5 22. Gagliardi G, Constine LS, Moiseenko V, et al. Radiation dose–volume effects in the
6
7 heart. *Int J Radiat Oncol Biol Phys* 2010;76(3):S77-S85.
- 8
9 23. Hyman L, Schachat AP, He Q, et al. Hypertension, cardiovascular disease, and age-
10
11 related macular degeneration. *Arch Ophthalmol* 2000;118(3):351-8.
- 12
13 24. Janeway TC. A clinical study of hypertensive cardiovascular disease. *Arch Intern Med*
14
15 1913;12(6):755-98.
- 16
17 25. Sowers JR, Epstein M, Frohlich ED. Diabetes, hypertension, and cardiovascular disease:
18
19 an update. *Hypertension* 2001;37(4):1053-9.
- 20
21 26. Wong TY, Klein R, Klein BE, et al. Retinal microvascular abnormalities and their
22
23 relationship with hypertension, cardiovascular disease, and mortality. *Surv Ophthalmol*
24
25 2001;46(1):59-80.
- 26
27 27. Armstrong GT, Oeffinger KC, Chen Y, et al. Modifiable risk factors and major cardiac
28
29 events among adult survivors of childhood cancer. *J Clin Oncol* 2013;31(29):3673.
- 30
31 28. Kirova Y, Tallet A, Aznar MC, et al. Radio-induced cardiotoxicity: From
32
33
34
35
36
37
38
39
40
41
42
43
44
45
46
47
48
49
50
51
52
53
54
55
56
57
58
59
60
61
62
63
64
65
66
67
68
69
70
71
72
73
74
75
76
77
78
79
80
81
82
83
84
85
86
87
88
89
90
91
92
93
94
95
96
97
98
99
100
101
102
103
104
105
106
107
108
109
110
111
112
113
114
115
116
117
118
119
120
121
122
123
124
125
126
127
128
129
130
131
132
133
134
135
136
137
138
139
140
141
142
143
144
145
146
147
148
149
150
151
152
153
154
155
156
157
158
159
160
161
162
163
164
165
166
167
168
169
170
171
172
173
174
175
176
177
178
179
180
181
182
183
184
185
186
187
188
189
190
191
192
193
194
195
196
197
198
199
200
201
202
203
204
205
206
207
208
209
210
211
212
213
214
215
216
217
218
219
220
221
222
223
224
225
226
227
228
229
230
231
232
233
234
235
236
237
238
239
240
241
242
243
244
245
246
247
248
249
250
251
252
253
254
255
256
257
258
259
260
261
262
263
264
265
266
267
268
269
270
271
272
273
274
275
276
277
278
279
280
281
282
283
284
285
286
287
288
289
290
291
292
293
294
295
296
297
298
299
300
301
302
303
304
305
306
307
308
309
310
311
312
313
314
315
316
317
318
319
320
321
322
323
324
325
326
327
328
329
330
331
332
333
334
335
336
337
338
339
340
341
342
343
344
345
346
347
348
349
350
351
352
353
354
355
356
357
358
359
360
361
362
363
364
365
366
367
368
369
370
371
372
373
374
375
376
377
378
379
380
381
382
383
384
385
386
387
388
389
390
391
392
393
394
395
396
397
398
399
400
401
402
403
404
405
406
407
408
409
410
411
412
413
414
415
416
417
418
419
420
421
422
423
424
425
426
427
428
429
430
431
432
433
434
435
436
437
438
439
440
441
442
443
444
445
446
447
448
449
450
451
452
453
454
455
456
457
458
459
460
461
462
463
464
465
466
467
468
469
470
471
472
473
474
475
476
477
478
479
480
481
482
483
484
485
486
487
488
489
490
491
492
493
494
495
496
497
498
499
500
501
502
503
504
505
506
507
508
509
510
511
512
513
514
515
516
517
518
519
520
521
522
523
524
525
526
527
528
529
530
531
532
533
534
535
536
537
538
539
540
541
542
543
544
545
546
547
548
549
550
551
552
553
554
555
556
557
558
559
560
561
562
563
564
565
566
567
568
569
570
571
572
573
574
575
576
577
578
579
580
581
582
583
584
585
586
587
588
589
590
591
592
593
594
595
596
597
598
599
600
601
602
603
604
605
606
607
608
609
610
611
612
613
614
615
616
617
618
619
620
621
622
623
624
625
626
627
628
629
630
631
632
633
634
635
636
637
638
639
640
641
642
643
644
645
646
647
648
649
650
651
652
653
654
655
656
657
658
659
660
661
662
663
664
665
666
667
668
669
670
671
672
673
674
675
676
677
678
679
680
681
682
683
684
685
686
687
688
689
690
691
692
693
694
695
696
697
698
699
700
701
702
703
704
705
706
707
708
709
710
711
712
713
714
715
716
717
718
719
720
721
722
723
724
725
726
727
728
729
730
731
732
733
734
735
736
737
738
739
740
741
742
743
744
745
746
747
748
749
750
751
752
753
754
755
756
757
758
759
760
761
762
763
764
765
766
767
768
769
770
771
772
773
774
775
776
777
778
779
780
781
782
783
784
785
786
787
788
789
790
791
792
793
794
795
796
797
798
799
800
801
802
803
804
805
806
807
808
809
810
811
812
813
814
815
816
817
818
819
820
821
822
823
824
825
826
827
828
829
830
831
832
833
834
835
836
837
838
839
840
841
842
843
844
845
846
847
848
849
850
851
852
853
854
855
856
857
858
859
860
861
862
863
864
865
866
867
868
869
870
871
872
873
874
875
876
877
878
879
880
881
882
883
884
885
886
887
888
889
890
891
892
893
894
895
896
897
898
899
900
901
902
903
904
905
906
907
908
909
910
911
912
913
914
915
916
917
918
919
920
921
922
923
924
925
926
927
928
929
930
931
932
933
934
935
936
937
938
939
940
941
942
943
944
945
946
947
948
949
950
951
952
953
954
955
956
957
958
959
960
961
962
963
964
965
966
967
968
969
970
971
972
973
974
975
976
977
978
979
980
981
982
983
984
985
986
987
988
989
990
991
992
993
994
995
996
997
998
999
1000
29. Mehta LS, Watson KE, Barac A, et al. Cardiovascular disease and breast cancer: where
these entities intersect: a scientific statement from the American Heart Association. *Circulation*
2018;137(8):e30-e66.
30. Banfill K, Giuliani M, Aznar M, et al. Cardiac toxicity of thoracic radiotherapy: existing
evidence and future directions. *J Thorac Oncol* 2021;16(2):216-27.

- 1
2
3 31. Ibrahim E-SH, Sosa A, Brown S-A, et al. Myocardial Contractility Pattern
4
5 Characterization in Radiation-Induced Cardiotoxicity Using Magnetic Resonance Imaging: A
6
7 Pilot Study with ContractiX. *Tomogr* 2023;9(1):36-49.
8
9
10 32. Abais-Battad JM, Saravia FL, Lund H, et al. Dietary influences on the Dahl SS rat gut
11
12 microbiota and its effects on salt-sensitive hypertension and renal damage. *Acta Physiol*
13
14 2021;232(4):e13662.
15
16
17 33. Mattson DL, Dwinell MR, Greene AS, et al. Chromosome substitution reveals the genetic
18
19 basis of Dahl salt-sensitive hypertension and renal disease. *Am J Physiol Renal Physiol*
20
21 2008;295(3):F837-F42.
22
23
24 34. Qu P, Hamada M, Ikeda S, et al. Time-course changes in left ventricular geometry and
25
26 function during the development of hypertension in Dahl salt-sensitive rats. *Hypertens Res*
27
28 2000;23(6):613-23.
29
30
31 35. Rapp J. Dahl salt-susceptible and salt-resistant rats. A review. *Hypertension*
32
33 1982;4(6):753-63.
34
35
36 36. Blinded for anonymity
37
38 37. Geurts AM, Mattson DL, Liu P, et al. Maternal diet during gestation and lactation
39
40 modifies the severity of salt-induced hypertension and renal injury in Dahl salt-sensitive rats.
41
42 *Hypertension* 2015;65(2):447-55.
43
44
45 38. Blinded for anonymity
46
47 39. Blinded for anonymity
48
49 40. Blinded for anonymity
50
51 41. Blinded for anonymity
52
53 42. Blinded for anonymity
54
55
56
57
58
59
60

- 1
2
3 43. Arts T, Prinzen FW, Delhaas T, et al. Mapping displacement and deformation of the heart
4 with local sine-wave modeling. *IEEE Trans Med Imaging* 2010;29(5):1114-23.
5
6
7
8 44. Blinded for anonymity
9
10 45. Bland JM, Altman D. Statistical methods for assessing agreement between two methods
11 of clinical measurement. *The lancet* 1986;327(8476):307-10.
12
13
14 46. Zietara A, Spires DR, Juffre A, et al. Knockout of the circadian clock protein PER1
15 (Period1) exacerbates hypertension and increases kidney injury in dahl salt-sensitive rats.
16 *Hypertension* 2022;79(11):2519-29.
17
18
19 47. Mayet J, Hughes A. Cardiac and vascular pathophysiology in hypertension. *Heart*
20 2003;89(9):1104-9.
21
22
23 48. Pfeffer MA, Pfeffer J, Mirsky I, et al. Cardiac hypertrophy and performance of Dahl
24 hypertensive rats on graded salt diets. *Hypertension* 1984;6(4):475-81.
25
26
27 49. Klotz S, Hay I, Zhang G, et al. Development of heart failure in chronic hypertensive Dahl
28 rats: focus on heart failure with preserved ejection fraction. *Hypertension* 2006;47(5):901-11.
29
30
31
32
33
34
35
36
37
38
39
40
41
42
43
44
45
46
47
48
49
50
51
52
53
54
55
56
57
58
59
60

Tables

Table 1. Comparison of cardiac and physiological parameters between sham and RT groups at baseline and 8-weeks after experiment. Parameters included systolic blood pressure (SBP in mmHg), diastolic blood pressure (DBP in mmHg), pulse rate (in bpm), end-diastolic volume (EDV in mL), end-systolic volume (ESV in mL), stroke volume (SV in mL), ejection fraction (EF %), mass (in g), and circumferential, radial, and longitudinal strains (Ecc, Err, and Ell %). Values are presented as mean \pm SD.

| | Baseline | | 8-weeks post-RT | | 12-weeks post-RT | |
|-------------|------------------|------------------|-----------------|------------------|------------------|-----------------|
| | Sham | RT | Sham | RT | Sham | RT |
| SBP (mmHg) | 232.5 \pm 12.0 | 223 \pm 37.4 | 280 \pm 8.5 | 223.3 \pm 38.5 | 306 | 181 \pm 54.6 |
| DBP (mm Hg) | 174 \pm 35.4 | 176.3 \pm 51.9 | 217 \pm 29.7 | 165.3 \pm 60.8 | 246 | 93.3 \pm 50.1 |
| Pulse (bpm) | 433 \pm 34 | 410 \pm 33 | 460 \pm 59 | 426 \pm 39 | 414 | 399 \pm 50 |
| EDV (mL) | 0.38 \pm 0.01 | 0.39 \pm 0.04 | 0.44 \pm 0 | 0.47 \pm 0.05 | 0.44 | 0.47 \pm 0.07 |
| ESV (mL) | 0.14 \pm 0.02 | 0.17 \pm 0.06 | 0.15 \pm 0.01 | 0.1 \pm 0.02 | 0.2 | 0.31 \pm 0.08 |
| SV (mL) | 0.24 \pm 0.03 | 0.25 \pm 0.04 | 0.29 \pm 0.01 | 0.38 \pm 0.05 | 0.24 | 0.17 \pm 0.01 |
| EF (%) | 63 \pm 7.1 | 64.5 \pm 11.7 | 66 \pm 2.8 | 80 \pm 3.6 | 56 | 36.5 \pm 7.8 |
| Mass (g) | 0.59 \pm 0.01 | 0.61 \pm 0.05 | 0.83 \pm 0.08 | 0.88 \pm 0.18 | 0.83 | 0.82 \pm 0.06 |
| Ecc (%) | -10.7 \pm 2.7 | -9.4 \pm 2.3 | -11 \pm 2.4 | -7.4 \pm 2.0 | -13.7 \pm 3.8 | -8.7 \pm 1.2 |
| Err (%) | 20.3 \pm 8.9 | 22.8 \pm 7.8 | 23 \pm 8.9 | 15.2 \pm 6.5 | 28.7 \pm 8.1 | 20.5 \pm 6.9 |
| Ell (%) | -15.9 \pm 5.0 | -14.5 \pm 6.3 | -15.2 \pm 4.1 | -13.5 \pm 4.2 | -15.8 \pm 5.4 | -10.3 \pm 3.6 |

Figures

Fig. 1. SS rats were fed high-salt diet for 4 weeks to develop hypertension before RT/sham treatment. Blood pressure measurements and MRI scans were conducted at baseline as well as 8- and 12-weeks post-RT or sham treatment. Histology analyses were conducted after last experiment or animal death.

Fig. 2. Dose distribution in different organs. Contours of lungs (right and left), heart, and spine visualized using MIM software in (A) transverse, (B) sagittal, and (C) coronal views. Regions receiving 97% of the prescribed dose were displayed in red, 80% in yellow, 60% in green, 40% in cyan, and 20% in purple. The dose volume histogram (DVHs) is presented in (D).

Fig. 3. Strain curves for the sham and RT groups show similar patterns in strain curves at baseline for circumferential, radial, and longitudinal strains. However, at 8-weeks post-RT, while the sham rats maintain comparable strain measurements, the irradiated rats show reduced strain magnitudes.

Fig. 4. Bland-Altman analysis illustrating consistency in strain for repeated measurements across multiple trials and observers. The diagrams (A-C) signify intra-observer and (D-F) indicate inter-observer measurements, denoting circumferential (A,D), radial (B,E), and longitudinal (C,F) strains. The majority of measurement differences are located within the $\text{mean} \pm 2\text{SD}$ range, implying low variability, thereby underlining the reliability and reproducibility of these strain measurements.

Fig. 5. The bar chart illustrates the survival status of rats in the sham and RT groups over a 12-week post-RT period. In the sham group, one rat was euthanized following a seizure at the end of the 11th week, and another rat was euthanized by the 12th week. In the RT group, two rats

1
2
3 developed heart failure and were euthanized, while another rat died, and one rat died during tail-
4 cuff blood pressure measurement.
5
6

7
8 Fig. 6. Histopathological changes in rat cardiac tissues observed using H&E staining (40×
9 magnification). A notable difference in staining intensity is observed, with the irradiated group
10 exhibiting a brighter pink hue, suggestive of a reduction in cytoplasmic proteins. In the sham
11 group (A-B), normal histoarchitecture is displayed, characterized by well-organized and
12 branched cardiac myofibers in the cardiomyocytes. In contrast, the irradiated rat (C-D) shows
13 increased nuclear size (black boxes), interstitial fibrosis and necrosis (purple boxes), increased
14 capillary density and presence of inflammatory cells (red boxes), as well as vacuolization of
15 sarcoplasm (blue boxes) in (D). Overall, the presence of inflammatory cells is more prominent in
16 the septal wall, while interstitial fibrosis and necrosis are more pronounced in the lateral wall.
17
18
19
20
21
22
23
24
25
26
27
28
29

30 Fig. 7. Masson's trichrome staining (40× magnification) of rat myocardial tissue from sham (A-
31 B) and irradiated tissues (C-D). The blue staining indicates the presence of collagen. Notably, the
32 irradiated group shows signs of tissue damage (white spot). In (E), the interstitial collagen
33 volume fraction is quantified for both sham and irradiated groups, with values expressed as mean
34 ± SD. The difference of interstitial collagen between the two groups was not statistically
35 significant, with a p-value of 0.72.
36
37
38
39
40
41
42
43

44 Fig. 8. Toluidine blue staining (40× magnification) of rat myocardial tissue from sham (A) and
45 irradiated groups (B). The dark blue staining indicates the mast cell (red arrows). The box plot
46 shows that there is a significant difference between two groups as p-value=0.01.
47
48
49
50

51 Fig. 9. Comparative analysis of various physiological metrics post-radiation therapy (RT)
52 between normotensive (NTN) and hypertensive (HTN) rats. Each plot depicts mean ± SD for (A)
53
54
55
56
57
58
59
60

1
2
3 ejection fraction (EF), (B) mass, (C) circumferential (Ecc), (D) radial (Err), and (E) longitudinal
4
5 (Ell) strains at three distinct time points: sham, 8-weeks post-RT, and 10/12 weeks post-RT. Blue
6
7 and red markers represent NTN and HTN rats, respectively.
8
9
10
11
12
13
14
15
16
17
18
19
20
21
22
23
24
25
26
27
28
29
30
31
32
33
34
35
36
37
38
39
40
41
42
43
44
45
46
47
48
49
50
51
52
53
54
55
56
57
58
59
60

For Peer Review Only

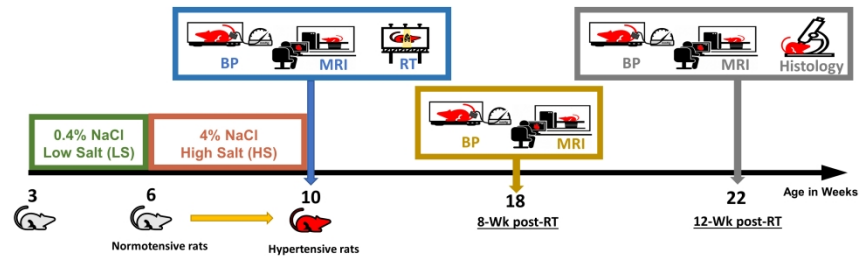


Fig. 1. SS rats were fed high-salt diet for 4 weeks to develop hypertension before RT/sham treatment. Blood pressure measurements and MRI scans were conducted at baseline as well as 8- and 12-weeks post-RT or sham treatment. Histology analyses were conducted after last experiment or animal death.

338x190mm (300 x 300 DPI)

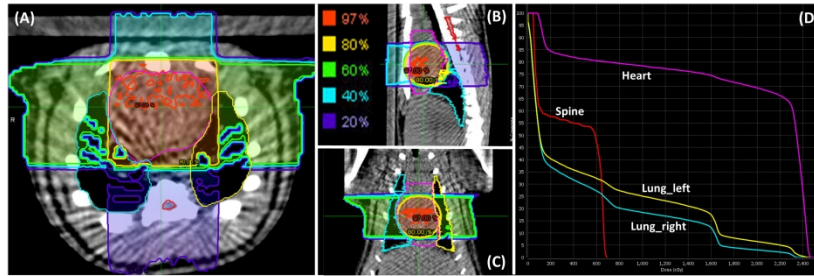


Fig. 2. Dose distribution in different organs. Contours of lungs (right and left), heart, and spine visualized using MIM software in (A) transverse, (B) sagittal, and (C) coronal views. Regions receiving 97% of the prescribed dose were displayed in red, 80% in yellow, 60% in green, 40% in cyan, and 20% in purple. The dose volume histogram (DVHs) is presented in (D).

338x190mm (300 x 300 DPI)

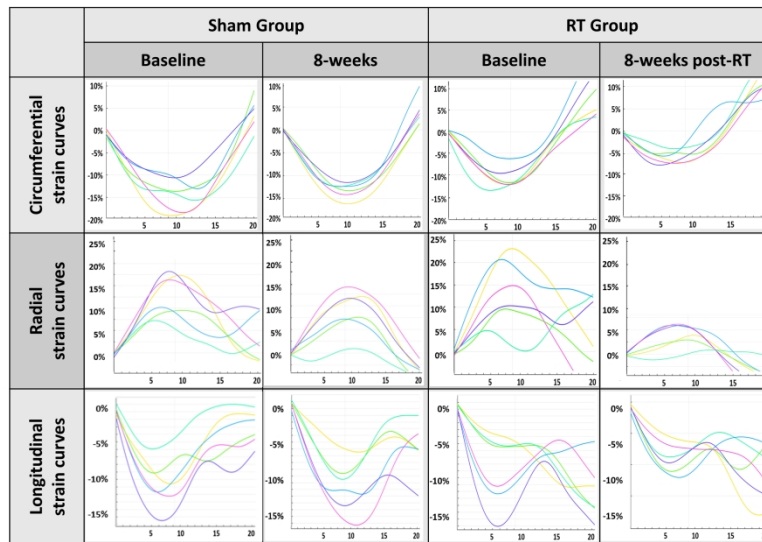


Fig. 3. Strain curves for the sham and RT groups show similar patterns in strain curves at baseline for circumferential, radial, and longitudinal strains. However, at 8-weeks post-RT, while the sham rats maintain comparable strain measurements, the irradiated rats show reduced strain magnitudes.

338x190mm (300 x 300 DPI)

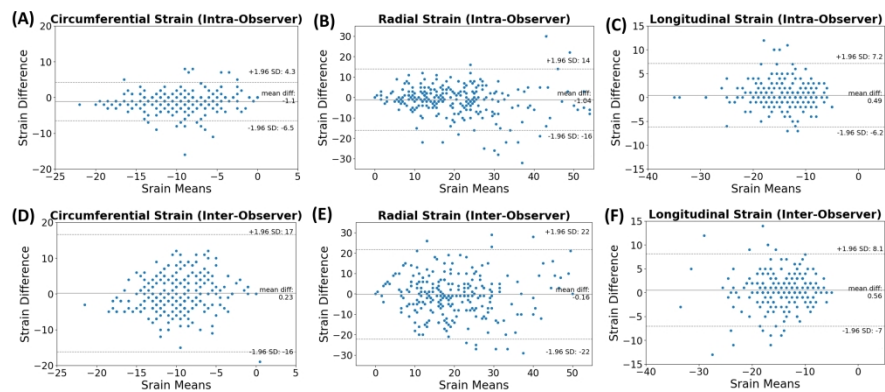


Fig. 4. Bland-Altman analysis illustrating consistency in strain for repeated measurements across multiple trials and observers. The diagrams (A-C) signify intra-observer and (D-F) indicate inter-observer measurements, denoting circumferential (A,D), radial (B,E), and longitudinal (C,F) strains. The majority of measurement differences are located within the mean \pm 2SD range, implying low variability, thereby underlining the reliability and reproducibility of these strain measurements.

338x190mm (300 x 300 DPI)

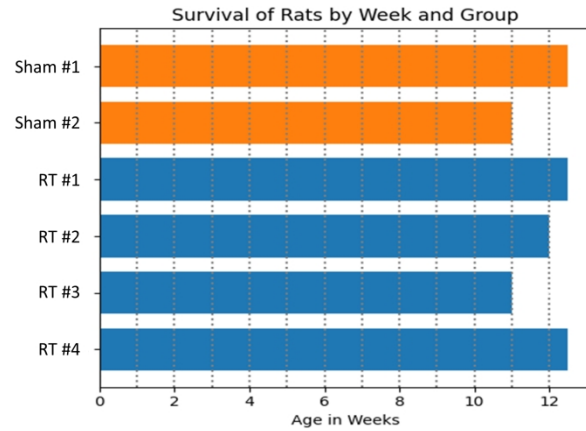


Fig. 5. The bar chart illustrates the survival status of rats in the sham and RT groups over a 12-week post-RT period. In the sham group, one rat was euthanized following a seizure at the end of the 11th week, and another rat was euthanized by the 12th week. In the RT group, two rats developed heart failure and were euthanized, while another rat died, and one rat died during tail-cuff blood pressure measurement.

338x190mm (300 x 300 DPI)

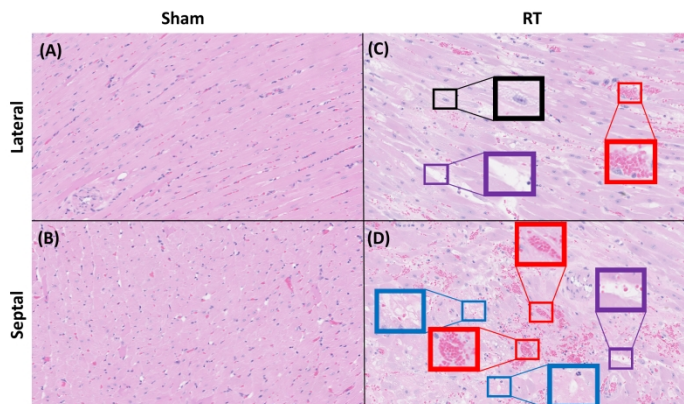


Fig. 6. Histopathological changes in rat cardiac tissues observed using H&E staining (40× magnification). A notable difference in staining intensity is observed, with the irradiated group exhibiting a brighter pink hue, suggestive of a reduction in cytoplasmic proteins. In the sham group (A-B), normal histoarchitecture is displayed, characterized by well-organized and branched cardiac myofibers in the cardiomyocytes. In contrast, the irradiated rat (C-D) shows increased nuclear size (black boxes), interstitial fibrosis and necrosis (purple boxes), increased capillary density and presence of inflammatory cells (red boxes), as well as vacuolization of sarcoplasm (blue boxes) in (D). Overall, the presence of inflammatory cells is more prominent in the septal wall, while interstitial fibrosis and necrosis are more pronounced in the lateral wall.

338x190mm (300 x 300 DPI)

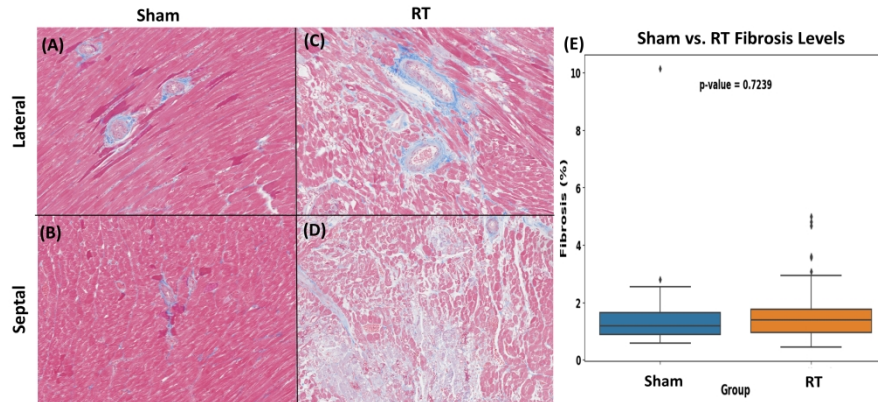


Fig. 7. Masson's trichrome staining (40× magnification) of rat myocardial tissue from sham (A-B) and irradiated tissues (C-D). The blue staining indicates the presence of collagen. Notably, the irradiated group shows signs of tissue damage (white spot). In (E), the interstitial collagen volume fraction is quantified for both sham and irradiated groups, with values expressed as mean \pm SD. The difference of interstitial collagen between the two groups was not statistically significant, with a p-value of 0.72.

338x190mm (300 x 300 DPI)

1
2
3
4
5
6
7
8
9
10
11
12
13
14
15
16
17
18
19
20
21
22
23
24
25
26
27
28
29
30
31
32
33
34
35
36
37
38
39
40
41
42
43
44
45
46
47
48
49
50
51
52
53
54
55
56
57
58
59
60

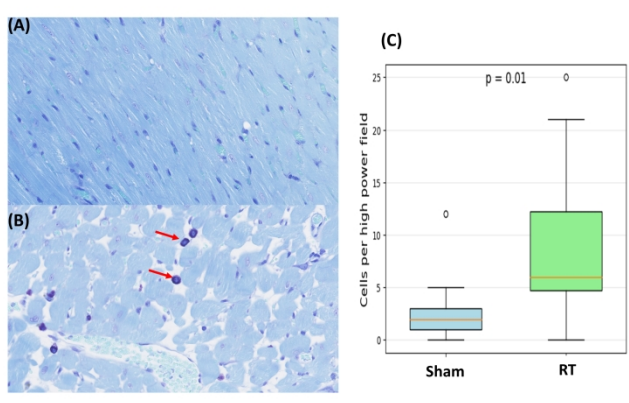


Fig. 8. Toluidine blue staining (40× magnification) of rat myocardial tissue from sham (A) and irradiated groups (B). The dark blue staining indicates the mast cell (red arrows). The box plot shows that there is a significant difference between two groups as p-value=0.01.

338x190mm (300 x 300 DPI)

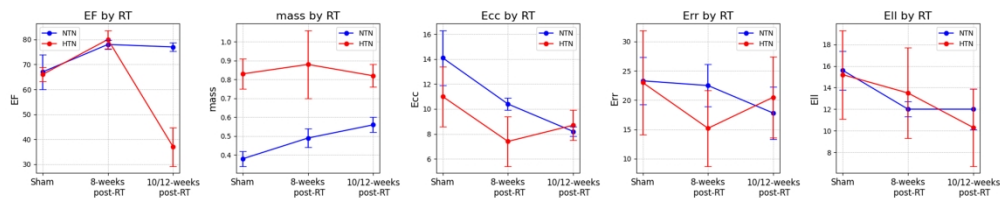


Fig. 9. Comparative analysis of various physiological metrics post-radiation therapy (RT) between normotensive (NTN) and hypertensive (HTN) rats. Each plot depicts mean \pm SD for (A) ejection fraction (EF), (B) mass, (C) circumferential (Ecc), (D) radial (Err), and (E) longitudinal (EII) strains at three distinct time points: sham, 8-weeks post-RT, and 10/12 weeks post-RT. Blue and red markers represent NTN and HTN rats, respectively.

338x190mm (300 x 300 DPI)